

# Effective Medium Theory of Filamentous Triangular Lattice

Xiaoming Mao,<sup>1</sup> Olaf Stenull,<sup>1</sup> and T. C. Lubensky<sup>1</sup>

<sup>1</sup>*Department of Physics and Astronomy, University of Pennsylvania, Philadelphia, PA 19104, USA*  
(Dated: November 9, 2011)

We present a new effective medium theory that can include bending as well as stretching forces, and we use it to calculate mechanical response of a diluted filamentous triangular lattice. In this lattice, bonds are central-force springs, and there are bending forces between neighboring bonds on the same filament. We investigate the diluted lattice in which each bond is present with a probability  $p$ . We find a rigidity threshold independent of filament bending rigidity at  $p_b \simeq 0.56$  and a crossover characterizing bending-, stretching-, and bend-stretch coupled elastic regimes controlled by the central-force isostatic point at  $p_{CF} = 2/3$  of the lattice when bending forces vanish.

PACS numbers: 87.16.Ka, 61.43.-j, 62.20.de, 05.70.Jk

## I. INTRODUCTION

Random elastic networks provide attractive and realistic models for the mechanical properties of materials as diverse as randomly packed spheres [1–3], network glasses [4–8], and biopolymer gels [9–20]. In their simplest form, these networks consist of nodes connected by central-force (CF) springs to on average  $z$  neighbors. They become more rigid as  $z$  increases, and they typically exhibit a CF rigidity percolation transition [21–23] from floppy, disconnected clusters to a sample spanning-cluster endowed with nonvanishing shear and bulk moduli at a threshold very close to the Maxwell isostatic limit [24, 25]  $z_{CF} = 2d$ , where  $d$  is the spatial dimension, at which the number of constraints imposed by the springs equals the number of degrees of freedom of isolated nodes. Generalized versions of these networks, appropriate for the description of network glasses [4, 5] and biopolymer gels [13–15], include bending forces favoring a particular angle between bonds (springs) incident on a given node. For a given value of  $z$ , networks with bending forces are more rigid than their CF-only counterparts, and they exhibit a rigidity transition at  $z = z_b < z_{CF}$ .

Though numerical calculations, including the pebble game [23, 26], have provided much of our knowledge about the properties of random elastic networks, effective medium theories (EMTs) [27–33] have provided simple and qualitatively correct descriptions of CF networks. EMTs [34–36] and heuristic approaches [37] that describe both bending and stretching forces have only recently been developed. Here we present details of the derivation of a bend-stretch EMT introduced in Ref. [35] and its application to a bond diluted triangular lattice, whose maximum coordination number is  $z_{\max} = 6$ . This lattice has bending and stretching forces modeled on those of biopolymer networks of filamentous semi-flexible polymers, characterized by one-dimensional stretching and bending moduli  $\mu$  and  $\kappa$  [13–15], respectively. Our EMT calculates the effective medium moduli  $\mu_m$  and  $\kappa_m$  as a function of  $\mu$  and  $\kappa$  and the probability  $p = z/6$  that a bond is occupied. Both the EMT bulk and shear modulus are proportional to  $\mu_m$ . When  $\kappa = 0$ , our EMT

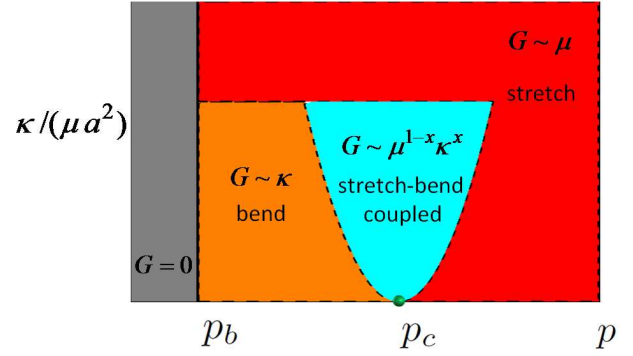


FIG. 1: (Color online) Phase diagram of the diluted filamentous triangular lattice showing the central-force and bending rigidity thresholds respectively at  $p = p_{CF}$  and  $p = p_b$ , the bending-dominated regime at small  $\kappa$  in the vicinity of  $p_b$ , the crossover bend-stretch regime near  $p_{CF}$ , and the stretching dominated regime at large  $\kappa$ .

reduces to that considered by others [29, 30] and successfully predicts a second-order CF rigidity threshold at  $z_{CF} = 4 < z_{\max}$  ( $p_{CF} = 2/3$ ) with  $\mu_m$  increasing linearly in  $p - p_{CF}$  near  $p_{CF}$  and approaching the undiluted triangular-lattice value of  $\mu$  at  $p = 1$ . When bending forces are introduced, our EMT predicts a new second-order bending dominated rigidity threshold at  $p = p_b = 0.56$  for all  $\kappa > 0$  near which  $\mu_m \sim \kappa(p - p_b)$  for  $\kappa/(\mu a^2) \ll 1$  and  $\mu_m \sim \mu(p - p_b)$  for  $\kappa/(\mu a^2) \gg 1$ , where  $a$  is the lattice spacing. Near  $p_{CF}$ ,  $\kappa$  is a relevant variable moving the system away from the CF rigidity critical point to a broad crossover regime [35, 37] in which  $\mu_m \sim \kappa^{1/2} \mu^{1/2}$  as shown in the phase diagram of Fig. 1. This crossover is analogous to that for the macroscopic conductivity in a resistor network in which bonds are occupied with resistors with conductance  $\sigma_>$  with probability  $p$  and with conductance  $\sigma_< < \sigma_>$  with probability  $1 - p$  [38].

Though the model we study has both stretching and bending forces, it differs in important ways from previously studied models for network glasses [4–8] and for filamentous gels [13–20]. The maximum coordination number for both of these systems is less than or equal

$2d$ , and thus neither has a CF rigidity transition for  $p < 1$  when there are no bending forces. As a result neither exhibits the bend-stretch crossover region near  $p_{\text{CF}}$  that our model exhibits. Network glasses are well modeled by a randomly diluted four-fold coordinated diamond lattice in which there is a bending-energy cost, characterized by a bending modulus  $\kappa$ , if the angle between any pair of bonds incident on a site deviates from the tetrahedral angle of  $109.5^\circ$ . The architecture of the undiluted diamond lattice (with  $z_{\text{max}} = 4 < 2d = 6$ ) is such that its shear modulus vanishes linearly with  $\kappa$  [7] and elastic response is nonaffine. When diluted, it exhibits a second-order rigidity transition from a state with bending-dominated nonaffine shear response to a state with no rigidity. As dilution decreases, rigidity is still controlled by  $\kappa$ , but response becomes less nonaffine.

Filamentous networks in two-dimensions are often described by the Mikado model [14–16] in which semi-flexible filaments of a given length  $L$  are deposited with random center-of-mass position and random orientation on a two-dimensional plane and the points where two filaments cross are joined in frictionless crosslinks. As in our model, there is no energy cost for the relative rotation of two rods about a crosslink, but there is an energy cost for bending the rods at crosslinks. This model is characterized by the ratio  $\eta \equiv L/l_c$  of the filament length  $L$  to the average mesh size, i.e., the average crosslink separation  $l_c > a$  along a filament, where  $a$  is a minimum cutoff length. In the limit  $\eta \rightarrow \infty$ , all filaments traverse the sample, and the system has finite,  $\kappa$ -independent shear and bulk moduli: There is effectively a CF rigidity transition at  $z = 4$  when  $\eta$  is decreased from infinity. There is a transition at  $\eta \approx 5.9$  to a rigid state with nonaffine response [14, 39], and there is a wide crossover region between  $\eta = \eta_c$  and  $\eta = \infty$  in which the shear modulus changes from being bend dominated, nonaffine, and nearly independent of  $\mu$  at small  $\eta$  to being stretch dominated, nearly affine, and nearly independent of  $\kappa$  at large  $\eta$ . Our EMT applied to the kagome lattice [40], whose maximum coordination number like that of the Mikado model is four, captures these crossovers. Interestingly,  $3d$  lattices composed of straight filaments with  $z_{\text{max}} = 4$  exhibit similar behavior [41]. When filaments are bent, however, elastic response in one case at least [20] is more like that of the diluted diamond lattice with the shear modulus vanishing with  $\kappa$  even at large  $L/l_c$  or  $z$  near 4.

External tensile stress (i.e., negative pressure) can cause a floppy lattice to become rigid [42]. Random internal stresses can do so as well in a phenomenon called tensegrity [25]. Thus a lattice with internal stresses may have a lower rigidity threshold than the same lattice with out internal stresses [20]. Systems such as network glasses can exhibit two rigidity transitions [8, 43]: a second-order transition from a floppy to a rigid but unstressed state followed closely by a first order transition to a rigid but stressed state. These effects are beyond the scope of your EMT and will not be treated.

The outline of our paper is as follows. Section II reviews properties of semi-flexible polymers and defines our model for the harmonic elasticity of crosslinked semi-flexible polymers on a triangular lattice; Sec. III sets up our effective medium theory; Sec. IV presents the results of this theory; and Sec. V compares our EMT with other versions of bend-stretch EMTs summarize our results. There are three appendices: App. B and App. C presents details of the derivation of crossover functions in the vicinity of  $p_{\text{CF}}$  and  $p_b$ , respectively; and App. D provides details on the estimation of  $p_b$  using generalized Maxwell counting arguments.

## II. FILAMENTOUS POLYMERS ON A TRIANGULAR LATTICE

The elastic energy of a single polymer is well described by the worm-like chain model [14, 44, 45] of an elastic rod

$$E = \frac{1}{2} \int_0^L ds \left[ \mu \left( \frac{dl(s)}{ds} \right)^2 + \kappa \left| \frac{d\hat{\mathbf{t}}(s)}{ds} \right|^2 \right], \quad (1)$$

where  $s$  is the arclength coordinate,  $L$  is the unstretched contour length of the polymer,  $dl(s)/ds$  and  $\hat{\mathbf{t}}(s)$  are, respectively, the extensional strain and unit tangent to the polymer at  $s$ , and  $\mu$  and  $\kappa$  are, respectively, the one-dimensional stretching and bending stiffnesses. Three length scales can be identified in this elastic energy. The first is the contour length of the polymers,  $L$ . The second,  $l_{\text{bend}} \equiv \sqrt{\kappa/\mu}$ , characterizes the relative strength of stretching and bending. For an elastic rod made of a homogeneous material,  $l_{\text{bend}}$  simply corresponds to the radius of the rod. The third length, the persistence length,  $l_p \equiv \kappa/(k_B T)$ , describes the scale of thermal undulations of the polymer at finite temperature. A fourth length, the mesh size  $l_c$  characterizing the connectivity of the network, can be identified for crosslinked polymer networks.

All these lengths participate in determining the elasticity of the polymer network above the rigidity threshold. Consider the force constants for harmonic distortions of an individual polymer segment of length  $l_c$ . At zero temperature, the force constant for longitudinal stretch of the segment is  $k_{\parallel,\mu} \sim \mu/l_c$ , and that for transverse deflection is  $k_{\perp} \sim \kappa/l_c^3$  (ignoring numerical factors). Thus the ratio  $l_{\text{bend}}/l_c \sim \sqrt{k_{\perp}/k_{\parallel,\mu}}$  characterizes the relative strength of bending and stretching of this particular segment of length  $l_c$  at low temperature. At finite temperature, thermal undulations of the filaments induce an effective series spring constant  $k_{\parallel,\text{th}} \sim k_B T l_p^2/l_c^4$  that results from pulling out thermal undulations [13, 15, 17]. At any given temperature, the physical parallel inverse spring constant is simply  $k_{\parallel}^{-1} = k_{\parallel,\mu}^{-1} + k_{\parallel,\text{th}}^{-1}$  so that  $k_{\parallel,\text{th}}$  dominates at high temperature and  $k_{\parallel,\mu}$  at low temperature. The ratio  $l_c/l_p \sim k_{\perp}/k_{\parallel}^{\text{th}}$  characterizes the relative ease of stretching vs. bending of this segment at high

temperature. Finally,  $L/l_c$  measures the connectivity of the network.

Here we investigate the harmonic elasticity of a model filamentous network on a bond-diluted triangular lattice with lattice constant  $a$  which is the mesh length  $l_c$ . Polymers correspond to lines of connected, occupied colinear bonds and crosslinks to sites at which two polymers to crosslinks. We use a model elastic energy obtained by discretizing the continuum model of Eq. (1) on our triangular lattice. To simplify notation, we use  $\mu/a \equiv \mu/l_c$  to represent the full  $k_{\parallel}$  rather than  $k_{\parallel,\mu}$  only, and we set  $k_{\perp} = \kappa/a^3 \equiv \kappa/l_c^3$ . Thus the elastic energy for a deformation that maps the position of lattice sites  $\ell$  from  $\mathbf{r}_{\ell}$  to  $\mathbf{R}_{\ell} = \mathbf{r}_{\ell} + \mathbf{u}_{\ell}$  can be written into the stretching part and the bending part

$$\begin{aligned} E &= E_s + E_b \\ E_s &= \frac{1}{2} \frac{\mu}{a} \sum_{\langle \ell, \ell' \rangle} g_{\ell, \ell'} (\mathbf{u}_{\ell\ell'} \cdot \hat{\mathbf{r}}_{\ell\ell'})^2, \\ E_b &= \frac{1}{2} \frac{\kappa}{a} \sum_{\langle \ell, \ell', \ell'' \rangle} g_{\ell, \ell'} g_{\ell', \ell''} \theta_{\ell\ell'\ell''}^2 \\ &= \frac{1}{2} \frac{\kappa}{a^3} \sum_{\langle \ell, \ell', \ell'' \rangle} g_{\ell, \ell'} g_{\ell', \ell''} [(\mathbf{u}_{\ell\ell'} - \mathbf{u}_{\ell'\ell''}) \times \hat{\mathbf{r}}_{\ell\ell'}]^2 \end{aligned} \quad (2a)$$

where  $\mathbf{u}_{\ell\ell'} \equiv \mathbf{u}_{\ell'} - \mathbf{u}_{\ell}$ ,  $\hat{\mathbf{r}}_{\ell\ell'}$  is the unit vector pointing from site  $\ell$  to nearest-neighbor (NN) site  $\ell'$  in the reference state (i.e., the state with  $\mathbf{u}_{\ell} = 0$  for all  $\ell$ ),  $g_{\ell, \ell'}$  is equal to one if the NN bond  $\langle \ell, \ell' \rangle$  is occupied and zero if the bond is empty,  $\theta_{\ell\ell'\ell''}$  is the angle between bond  $\langle \ell, \ell' \rangle$  and  $\langle \ell', \ell'' \rangle$  in the deformed state as shown in Fig. 2(b), with  $\mathbf{r}_{\ell}$ ,  $\mathbf{r}_{\ell'}$ , and  $\mathbf{r}_{\ell''}$  along a line. The stretch spring constant  $\mu/a$  is defined on each NN bond, and the bending constant  $\kappa/a^3$  is defined for each next-nearest-neighbor (NNN) bond along a straight line (i.e., in the same filament). We have used the fact that the filaments are straight ( $\theta = 0$ ) in the reference state so  $\hat{\mathbf{r}}_{\ell\ell'} = \hat{\mathbf{r}}_{\ell'\ell''}$ . There is an important distinction, which will be of importance in our development of an effective-medium theory, between the stretching energy  $E_s$  and the bending energy  $E_b$ . The former is a sum of energies on individual bonds  $\langle \ell, \ell' \rangle$  connecting NN sites  $\ell$  and  $\ell'$ , whereas the latter is a sum of energies on the pair of connected bonds  $\langle \ell, \ell' \rangle$  and  $\langle \ell', \ell'' \rangle$  or, alternatively, on a *phantom* NNN bond connecting sites  $\ell$  and  $\ell''$ . This phantom bond is not an independent connection; it is only present and resists bending if both bonds  $\langle \ell, \ell' \rangle$  and  $\langle \ell', \ell'' \rangle$  are occupied. We will have more to say about this in Sec. V when we discuss the relation of our work to that of Refs. [34] and [36].

Upon dilution, each of the bonds is present with a probability  $p$ , and the resulting lattice corresponds to a random network of semiflexible filaments of finite random lengths  $L$ , whose average as a function of  $p$  is  $\langle L \rangle = 1/(1-p)$  [35].

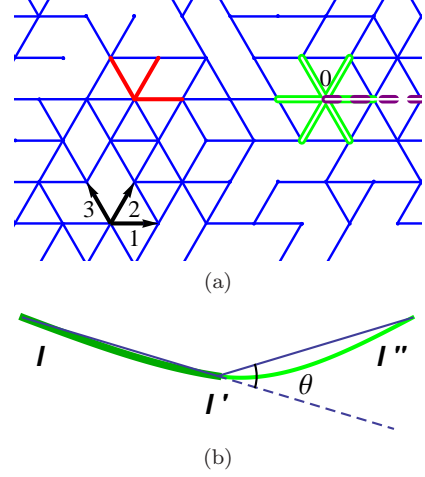


FIG. 2: (color online) (a) Filamentous triangular lattice with bonds randomly occupied with probability  $p$ . The unit vectors  $\hat{\mathbf{e}}_1^{\parallel}, \hat{\mathbf{e}}_2^{\parallel}, \hat{\mathbf{e}}_3^{\parallel}$  are marked by “1, 2, 3”, the 3 stretch energy vectors  $\mathbf{B}_n^s$  are marked by the 3 red single lines, and the 3 bending energy vectors  $\mathbf{B}_n^b$  are marked by the 3 green double lines. The purple dashed double line marks the bending vector  $\mathbf{B}_4^s$  if the origin is marked by 0. (b) Illustration of the bending energy term 2b. The green curves correspond to the filament by requiring that it has to pass through lattice sites  $\ell, \ell', \ell''$ . The ratio of the bending elastic modulus of the darker green segment and the lighter green segment is  $\kappa_1/\kappa_2 = 3$ . The bending energy term at site  $\ell'$  is proportional to  $2(\frac{1}{\kappa_1} + \frac{1}{\kappa_2})^{-1}$  determined by minimizing the elastic energy.

### III. EFFECTIVE MEDIUM THEORY

We study the elasticity of our network using an effective-medium approximation [27, 28] that maps the random network to an effective-medium uniform lattice in which all bonds are present with respective stretching and bending constant  $\mu_m$  and  $\kappa_m$ , which are determined self-consistently. This approximation has been shown to be a powerful tool for the calculation of properties of random systems, from the electronic structure of alloys [27, 46] to the elasticity of random networks [29, 47]. It is straightforward to write the elastic energy  $\Delta E$  of this uniform effective medium lattice in terms of the dynamical matrix,  $\mathbf{D}_{\mathbf{q}}$ :

$$\Delta E = \frac{1}{2N^2} \sum_{\mathbf{q}} \mathbf{u}_{-\mathbf{q}} \cdot \mathbf{D}_{\mathbf{q}} \cdot \mathbf{u}_{\mathbf{q}}, \quad (3)$$

where the Fourier transform of  $\mathbf{u}$  is defined as

$$\mathbf{u}_{\mathbf{q}} = \sum_{\ell} \mathbf{u}_{\ell} e^{-i\mathbf{q} \cdot \mathbf{r}_{\ell}}, \quad \mathbf{u}_{\ell} = \frac{1}{N} \sum_{\mathbf{q}} \mathbf{u}_{\mathbf{q}} e^{i\mathbf{q} \cdot \mathbf{r}_{\ell}}, \quad (4)$$

and the dynamical matrix can be written as a sum of the outer product of the stretching and bending bond vectors

$$\mathbf{D}_{\mathbf{q}}(\mu_m, \kappa_m) = \frac{\mu_m}{a} \sum_{n=1}^3 \mathbf{B}_{n,\mathbf{q}}^s \mathbf{B}_{n,-\mathbf{q}}^s + \frac{\kappa_m}{a^3} \sum_{n=1}^3 \mathbf{B}_{n,\mathbf{q}}^b \mathbf{B}_{n,-\mathbf{q}}^b \quad (5)$$

where

$$\begin{aligned}\mathbf{B}_{n,\mathbf{q}}^s &= (1 - e^{-i\mathbf{q}\cdot\hat{\mathbf{e}}_n^\parallel})\hat{\mathbf{e}}_n^\parallel \\ \mathbf{B}_{n,\mathbf{q}}^b &= 2(1 - \cos(\mathbf{q}\cdot\hat{\mathbf{e}}_n^\parallel))\hat{\mathbf{e}}_n^\perp\end{aligned}\quad (6)$$

with  $\hat{\mathbf{e}}_n^\parallel$  the unit vector along bond  $n$  defined in Fig. 2(a) and  $\hat{\mathbf{e}}_n^\perp$  the unit vector perpendicular to  $\hat{\mathbf{e}}_n^\parallel$ . The sum is over the three bonds in one unit cell for  $\mathbf{B}^s$  or the three pairs of bonds for  $\mathbf{B}^b$ . We used the periodicity of the lattice to obtain this translationally invariant form as will become clear when we discuss the perturbation calculation below.

In the long-wavelength limit, the energy of our undiluted harmonic triangular lattice reduces to the elastic energy of an isotropic  $2d$  medium,

$$E = \int d^2x \left[ \frac{\hat{\lambda}}{2} (\text{Tr}\underline{u})^2 + \hat{\mu} \text{Tr}\underline{u}^2 \right], \quad (7)$$

where  $\underline{u}$  is the linearized symmetric Cauchy strain tensor with Cartesian components  $u_{ij}$ ,  $\hat{\lambda}$  and  $\hat{\mu}$  are the Lamé coefficients,  $\hat{\lambda} = \hat{\mu} = (\sqrt{3}/4)(\mu/a)$ , which depend only on  $\mu$  and not on  $\kappa$ . The bending constant  $\kappa$  only appears in the  $O(q^4)$  terms in this elastic energy.

The effective medium is characterized by a stretch spring constant  $\mu_m$  that has the same value on every  $NN$  bond and a bending constant  $\kappa_m$  that has the same value on every  $NNN$  phantom bond along a line. The self-consistency conditions determining  $\mu_m$  and  $\kappa_m$  are treated differently. In the dilution procedure, bonds are removed with probability  $1 - p$ . In the process, a bond with spring constant  $\mu_m$  is replaced by one with spring constant 0, and the scattering potential relative to the effective-medium state arising from this replacement is proportional to  $\mu - \mu_m$  if the bond is occupied and  $-\mu_m$  if it is vacant. Bending couples  $NNN$  sites along a line and must be treated differently. Consider two bonds along a line,  $\langle \ell\ell' \rangle$  and  $\langle \ell'\ell'' \rangle$ , sharing a common site  $\ell'$  and composed of rods with respective one-dimensional bending moduli  $\kappa_1$  and  $\kappa_2$  defined in Eq. (1). The phantom bending bond connecting  $NNN$  sites is now a composite one [Fig. 2(b)] consisting of two  $NN$  bonds tied together at the intermediate site  $\ell'$ . A direct calculation of the minimum bending energy [Eq. (1) with  $dl/ds = 0$ ], for fixed bending angle  $\theta$ , in this composite bond yields an effective bending constant  $\kappa_{\text{eff}} = 2(\kappa_1^{-1} + \kappa_2^{-1})^{-1}$  that reduces to  $\kappa_1$  if  $\kappa_1 = \kappa_2$  and 0 if either  $\kappa_1$  or  $\kappa_2 = 0$ . An example of the energy minimizing bending configuration is shown in Fig. 2(b). We derive the effective bending constant of this composite bond in App. A.

Consider sites  $\ell_0, \ell_1, \ell_2$ , and  $\ell_3$  along a line. The removal of the central bond  $\langle \ell_1\ell_2 \rangle$  will modify the bending modulus of that bond and thus the bending energy of both  $NNN$  phantom bonds  $\langle \ell_0\ell_2 \rangle$  and  $\langle \ell_1\ell_3 \rangle$  containing the  $NN$  bond  $\langle \ell_1\ell_2 \rangle$ . Thus, the bending modulus relative to that of the effective medium of both these  $NNN$

phantom bonds is  $\kappa_c(\kappa_s) - \kappa_m$ , where

$$\kappa_c = 2\left(\frac{1}{\kappa_s} + \frac{1}{\kappa_m}\right)^{-1}, \quad (8)$$

where  $\kappa_s = 0$  if the bond  $\langle \ell_1\ell_2 \rangle$  is absent and  $\kappa_s = \kappa$  if it is present. In the latter case  $\kappa_c = 2\kappa\kappa_m/(\kappa + \kappa_m)$  is a nonlinear function of  $\kappa$  and  $\kappa_m$ .

With these rules, we can write the perturbation to the dynamical matrix resulting from the replacement of one bond as

$$\begin{aligned}\mathbf{V}_{\mathbf{q},\mathbf{q}'}(\mu_s, \kappa_s) &= a^{-1}(\mu_s - \mu_m)\mathbf{B}_{1,\mathbf{q}}^s\mathbf{B}_{1,-\mathbf{q}'}^s \\ &+ a^{-3}(\kappa_c(\kappa_s) - \kappa_m)\mathbf{B}_{1,\mathbf{q}}^b\mathbf{B}_{1,-\mathbf{q}'}^b \\ &+ a^{-3}(\kappa_c(\kappa_s) - \kappa_m)\mathbf{B}_{4,\mathbf{q}}^b\mathbf{B}_{4,-\mathbf{q}'}^b, \quad (9)\end{aligned}$$

where we have chosen to replace the bond between the two sites  $\mathbf{r}_0 = 0$  and  $\mathbf{r}_1 = a\hat{\mathbf{e}}_1^\parallel$  for convenience. The vector  $\mathbf{B}_{4,\mathbf{q}}^b \equiv e^{-i\mathbf{q}\cdot\hat{\mathbf{e}}_1^\parallel}\mathbf{B}_{1,\mathbf{q}}^b$  represents the bending of the bond pair connecting sites  $\mathbf{r}_0 = 0$ ,  $\mathbf{r}_1 = a\hat{\mathbf{e}}_1^\parallel$ , and  $2\mathbf{r}_1$ , as shown in Fig. 2(a). The replaced stretching spring constant  $\mu_s$  and bending modulus  $\kappa_s$  follow the probability distribution

$$\begin{aligned}P(\mu_s) &= p\delta(\mu_s - \mu) + (1 - p)\delta(\mu_s) \\ P(\kappa_s) &= p\delta(\kappa_s - \kappa) + (1 - p)\delta(\kappa_s).\end{aligned}\quad (10)$$

In this study we are primarily concerned with the static properties of the effective medium, which is characterized by the zero-frequency phonon Green's function

$$\mathbf{G}_{\mathbf{q}} = -\mathbf{D}_{\mathbf{q}}^{-1}. \quad (11)$$

When one bond of the effective medium is replaced,  $\mathbf{D} \rightarrow \mathbf{D} + \mathbf{V}$ , and the Green's function is given by the following expansion

$$\begin{aligned}\mathbf{G}_{\mathbf{q},\mathbf{q}'}^V &= (\mathbf{I} - \mathbf{G} \cdot \mathbf{V})_{\mathbf{q},\mathbf{q}'}^{-1} \cdot \mathbf{G}_{\mathbf{q}'} \\ &= N\delta_{\mathbf{q},\mathbf{q}'}\mathbf{G}_{\mathbf{q}} + \mathbf{G}_{\mathbf{q}} \cdot \mathbf{T}_{\mathbf{q},\mathbf{q}'} \cdot \mathbf{G}_{\mathbf{q}'}, \quad (12)\end{aligned}$$

where the  $\mathbf{T}$  matrix is

$$\begin{aligned}\mathbf{T}_{\mathbf{q},\mathbf{q}'} &\equiv \mathbf{V}_{\mathbf{q},\mathbf{q}'} + \frac{1}{N} \sum_{\mathbf{q}_1} \mathbf{V}_{\mathbf{q},\mathbf{q}_1} \cdot \mathbf{G}_{\mathbf{q}_1} \cdot \mathbf{V}_{\mathbf{q}_1,\mathbf{q}'} \\ &+ \frac{1}{N^2} \sum_{\mathbf{q}_1, \mathbf{q}_2} \mathbf{V}_{\mathbf{q},\mathbf{q}_1} \cdot \mathbf{G}_{\mathbf{q}_1} \cdot \mathbf{V}_{\mathbf{q}_1,\mathbf{q}_2} \cdot \mathbf{G}_{\mathbf{q}_2} \cdot \mathbf{V}_{\mathbf{q}_2,\mathbf{q}'} \\ &+ \dots\end{aligned}\quad (13)$$

In EMT, the effective-medium elastic parameters  $\mu_m$  and  $\kappa_m$  are determined by requiring that the disorder average of  $\mathbf{G}^V$  be equal to  $\mathbf{G}$  of the effective-medium uniform lattice with stretching and bending constants  $\mu_m$  and  $\kappa_m$ . This is equivalent to requiring that the disorder average,

$$p\mathbf{T}|_{\mu_s=\mu, \kappa_s=\kappa} + (1 - p)\mathbf{T}|_{\mu_s=0, \kappa_s=0} = 0, \quad (14)$$

of the  $\mathbf{T}$ -matrix vanish.



In traditional EMT with no bending modulus, the only elastic parameter is the stretching spring constant  $\mu_m$ , and one can simplify the  $\mathbf{T}$  matrix by making use of the equation

$$\frac{1}{N} \sum_{\mathbf{q}_1} \mathbf{V}_{\mathbf{q}, \mathbf{q}_1} \cdot \mathbf{G}_{\mathbf{q}_1} \cdot \mathbf{V}_{\mathbf{q}_1, \mathbf{q}'} = -a^{-1}(\mu_s - \mu_m) \mathbf{V}_{\mathbf{q}, \mathbf{q}'} f(\mu_m), \quad (15)$$

where  $f$  is a scalar function. However, in this case with bending energy terms, which couple the replaced bond with two neighboring bonds, the product  $\mathbf{V}_{\mathbf{q}, \mathbf{q}_1} \mathbf{G}_{\mathbf{q}_1} \mathbf{V}_{\mathbf{q}_1, \mathbf{q}'}$

contains cross terms such as  $\mathbf{B}_{1, \mathbf{q}}^b \mathbf{B}_{1, -\mathbf{q}_1}^b \cdot \mathbf{G}_{\mathbf{q}_1} \cdot \mathbf{B}_{4, \mathbf{q}_1}^b \mathbf{B}_{4, -\mathbf{q}'}^b$  which do not reduce to  $\mathbf{V}_{\mathbf{q}, \mathbf{q}'} f$ .

Here we develop a new variation of the EMT to solve this self-consistency equation (14). In this method, we introduce an effective medium coupling between neighboring bond pairs along filaments that share a bond, e.g.,  $\mathbf{B}_1^b \mathbf{B}_4^b$ , with a coupling constant  $\lambda_m$ , to account for the cross terms discussed above. For convenience we express the self-consistency equation in the space defined by the basis  $\{|\mathbf{B}_1^s\rangle, |\mathbf{B}_1^b\rangle, |\mathbf{B}_4^s\rangle\}$ , in which the perturbation is

$$\tilde{\mathbf{V}}(\mu_s, \kappa_s) = \begin{pmatrix} (\mu_s - \mu_m)/a & 0 & 0 \\ 0 & (\kappa_c(\kappa_s) - \kappa_m)/a^3 & -\lambda_m/a^3 \\ 0 & -\lambda_m/a^3 & (\kappa_c(\kappa_s) - \kappa_m)/a^3 \end{pmatrix}, \quad (16)$$

where the tilde marks the addition of the  $\lambda_m$  coupling. Cross terms such as  $\mathbf{B}_1^s \mathbf{B}_1^b$  vanish because they violate the space inversion symmetry,  $\mathbf{q} \rightarrow -\mathbf{q}$ .

On the other hand, the  $\lambda_m$  coupling terms also need to be added to the dynamical matrix

$$\begin{aligned} \tilde{\mathbf{D}}_{\mathbf{q}}(\mu_m, \kappa_m) &= \mathbf{D}_{\mathbf{q}}(\mu_m, \kappa_m) \\ &+ a^{-3} \lambda_m \sum_{n=1}^3 2 \cos(\mathbf{q} \cdot \hat{\mathbf{e}}_n^{\parallel}) \mathbf{B}_{n, \mathbf{q}}^b \mathbf{B}_{n, -\mathbf{q}}^b, \end{aligned} \quad (17)$$

and the Green's function is modified to  $\tilde{\mathbf{G}} = -\tilde{\mathbf{D}}^{-1}$ .

By writing the  $\mathbf{T}$  matrix as

$$\tilde{\mathbf{T}} = (\tilde{\mathbf{V}}^{-1} - \tilde{\mathbf{G}})^{-1}, \quad (18)$$

the self-consistency equation takes the form

$$p[\tilde{\mathbf{V}}^{-1}(\mu, \kappa) - \tilde{\mathbf{G}}]^{-1} + (1-p)[\tilde{\mathbf{V}}^{-1}(0, 0) - \tilde{\mathbf{G}}]^{-1} = 0 \quad (19)$$

Multiplying by  $(\tilde{\mathbf{V}}^{-1}(\mu, \kappa) - \tilde{\mathbf{G}})$  on the left and by  $(\tilde{\mathbf{V}}^{-1}(0, 0) - \tilde{\mathbf{G}})$  on the right we arrive at

$$p\tilde{\mathbf{V}}^{-1}(0, 0) + (1-p)\tilde{\mathbf{V}}^{-1}(\mu, \kappa) - \tilde{\mathbf{G}} = 0. \quad (20)$$

This equation can be solved in the space of  $\{|\mathbf{B}_1^s\rangle, |\mathbf{B}_1^b\rangle, |\mathbf{B}_4^s\rangle\}$ . To do this we define the notation

$$\mathbf{H}(b_m, l_m) \equiv -\frac{\mu_m}{a} \tilde{\mathbf{G}}(\mu_m, \kappa_m, \lambda_m). \quad (21)$$

From the definition of  $\tilde{\mathbf{G}}$  it is straightforward to see that  $H$  only depends on the ratios  $b_m \equiv \kappa_m/\mu_m$  and  $l_m \equiv \lambda_m/\mu_m$ . We then project  $\mathbf{H}$  to this basis

$$\mathbf{H}(b_m, l_m) = \begin{pmatrix} H_1 & 0 & 0 \\ 0 & H_2 & H_3 \\ 0 & H_3 & H_2 \end{pmatrix}, \quad (22)$$

with

$$H_1 \equiv \langle \mathbf{B}_1^s | \mathbf{H} | \mathbf{B}_1^s \rangle \equiv \int_{\text{1BZ}} \frac{d^2 \mathbf{q}}{4\pi^2/v} \mathbf{B}_{1, \mathbf{q}}^s \cdot \mathbf{H}_{\mathbf{q}} \cdot \mathbf{B}_{1, \mathbf{q}}^s \quad (23)$$

where we have defined the inner product as an integral over the first Brillouin zone and the factor  $v$  is the volume of each unit cell in real space. Similarly,  $H_2 \equiv \langle \mathbf{B}_1^b | \mathbf{H} | \mathbf{B}_1^b \rangle$  and  $H_3 \equiv \langle \mathbf{B}_1^b | \mathbf{H} | \mathbf{B}_4^b \rangle$ . As we mentioned earlier, couplings between  $\mathbf{B}^s$  and  $\mathbf{B}^b$  terms vanish in the dynamical matrix  $\tilde{\mathbf{D}}$ , because  $\tilde{\mathbf{D}}$  is even in momentum  $\mathbf{q}$ . As a result, the projections  $\langle \mathbf{B}_1^s | \mathbf{H} | \mathbf{B}_1^b \rangle = 0$  and  $\langle \mathbf{B}_1^s | \mathbf{H} | \mathbf{B}_4^b \rangle = 0$ . This is consistent with the vanishing cross term between  $\mathbf{B}^s$  and  $\mathbf{B}^b$  in  $\tilde{\mathbf{V}}^{-1}$ . Thus the self-consistency equation (20) closes, providing 3 independent equations for the 3 unknowns  $(\mu_m, \kappa_m, \lambda_m)$  whose solution we will discuss in the next section.

#### IV. EMT RESULTS

Numerical solutions to Eq. (20) for any value of  $\kappa/\mu$  are easily calculated, and the results for the effective medium elastic parameters, and the results are plotted in Figs. 3, 4. There are several properties of these plots that are worthy of note:

1.  $\mu_m$  vanishes at the  $CF$  Maxwell rigidity threshold  $p_{\text{CF}} = 2/3$  when  $\kappa = 0$  and at  $p = p_b = 0.56$  for all  $\kappa > 0$ . Simulations of the same model yield that  $p_{\text{CF}} \simeq 0.659$  and  $p_b \simeq 0.445$  [36]. (In App. D, we present a variation of the Maxwell floppy mode count to estimate the rigidity threshold in presence of filament bending stiffness and obtain  $p_b \simeq 0.448$  in good agreement with simulation results.)
2. Increasing  $\kappa$  increases  $\mu_m$  for all  $p$  except at  $p = p_b$ .
3. For small  $\kappa/(\mu a^2)$ , there is an interesting and nontrivial crossover near  $p_{\text{CF}}$  whereas for large

$\kappa/(\mu a^2)$ , memory of the CF threshold is effectively lost and  $\mu_m$  rapidly reaches value near its saturation value  $\mu$  for  $p > p_b$ .

4.  $\kappa_m$  vanishes as  $p \rightarrow p_b$  and rises smoothly to its saturation value  $\kappa$  without any evidence of crossover behavior near  $p_{CF}$ .
5.  $\lambda_m$  vanishes at  $p_b$  and in the undiluted lattice ( $p = 1$ ), which it must by construction. It exhibits crossover behavior near  $p = p_{CF}$  for small  $\kappa/(\mu a^2)$ .

In what follows, we discuss analytic expressions derived from Eq. (20) that captures these behaviors.

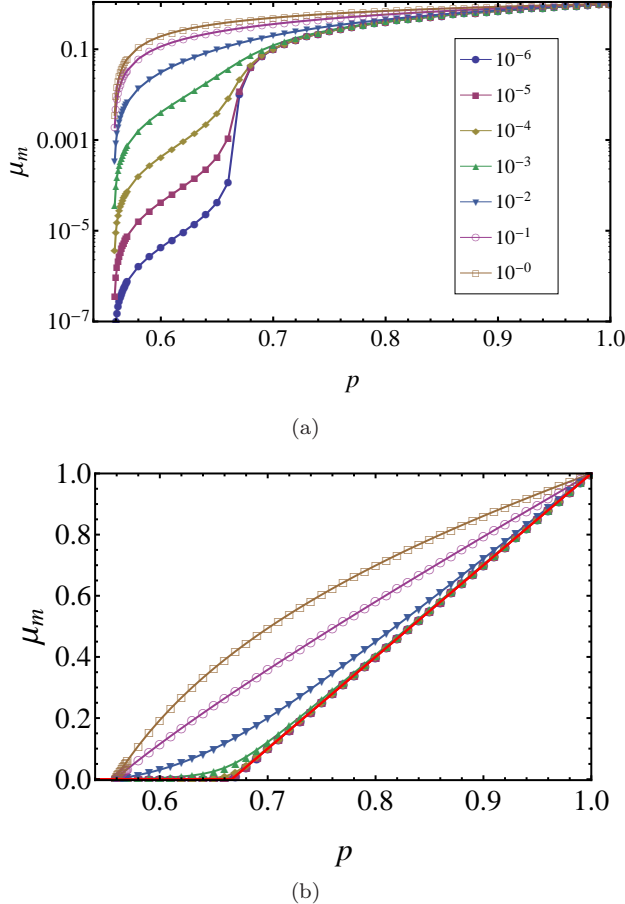


FIG. 3: (color online) (a) Semi-log plot for the EMT solution  $\mu_m$  as a function of  $p$  for  $\mu = 1$  and  $\kappa = 1, 10^{-1}, 10^{-2}, 10^{-3}, 10^{-4}, 10^{-5}, 10^{-6}$  from top to bottom, as indicated in the legend. (b) Linear plot of  $\mu_m$  as a function of  $p$ , with parameters and color code the same as in (a). The red solid line indicates  $\mu_m$  for the case of a central force triangular lattice ( $\kappa = 0$ ).

#### A. Behavior near $p = p_b$

We begin with behavior near  $p_b$ . As detailed in App. C,  $\mu_m$  approaches zero linearly in  $\delta p \equiv p - p_b$  for all values

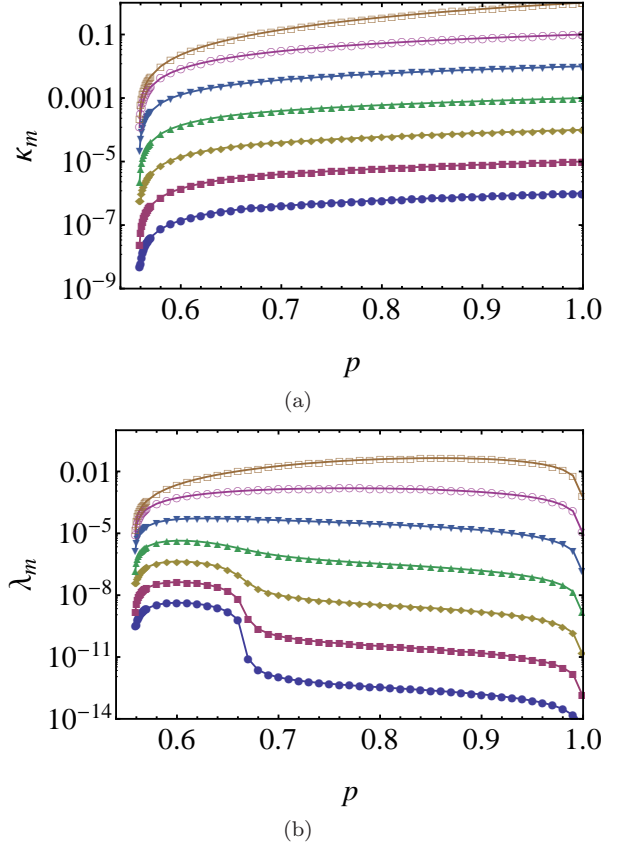


FIG. 4: (color online) The EMT solution for  $\kappa_m$  (a) and  $\lambda_m$  (b). Parameters and color code are the same as in Fig. 3.

of  $\kappa$  as

$$\mu_m = \frac{\kappa}{a^2} \frac{c_2 \delta p}{\kappa/(\mu a^2) + c_1}, \quad (24)$$

where  $c_1$  and  $c_2$  are constants determined by the architecture of the lattice and are independent of  $p$  or  $\kappa/(\mu a^2)$ , and both  $\kappa_m$  and  $\lambda_m$  are linearly proportional to  $\mu_m$  for small  $\delta p$  with corrections of order  $\delta p^2$ . The linear dependence on  $\delta p$  of these quantities is what one would expect from an EMT. The prefactor, shows important dependence on  $\kappa$ . When  $\kappa/(\mu a^2) \ll 1$ ,  $\mu_m$  is linearly proportional to  $\kappa$  and independent of  $\mu$  whereas for  $\kappa/(\mu a^2) \gg 1$ ,  $\mu_m$  is linearly proportional to  $\mu$  and independent of  $\kappa$ . Thus the system behaves as if the it consists of a “bending spring” with spring constant  $\kappa/a^3$  in series with a stretching spring with spring constant  $\mu/a$ . This result explains the increase in slope of  $\mu_m$  at  $p_b$  with increasing  $\kappa$  and the saturation of  $\mu_m$  for  $p$  near  $p_b$  for large  $\kappa/(\mu a^2)$ . In Fig. 5 we show a comparison between the asymptotic solution (24) and the numerical solutions of the EMT equations, which agree very well.

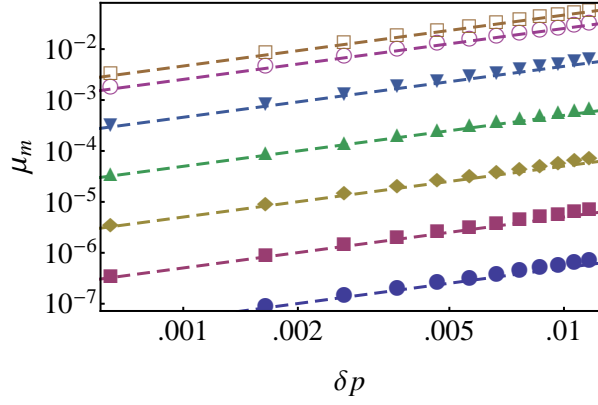


FIG. 5: (Color online) Asymptotic solution (dashed lines) and numerical solutions (data points) of  $\mu_m$  near  $p_b$ . Parameters and color code are the same as in Fig. 3.

### B. Behavior near $p = p_{CF}$

We show in App. B that in the vicinity of the CF rigidity threshold at small  $\kappa$ , the effective medium spring constants for given  $\Delta p \equiv p - p_{CF}$  adopt the scaling forms

$$\mu_m = \mu |\Delta p|^{t_1} g_{1,\pm} \left( \frac{\kappa}{a^2 \mu |\Delta p|^\phi} \right), \quad (25a)$$

$$\kappa_m = \mu |\Delta p|^{t_2} g_{2,\pm} \left( \frac{\kappa}{a^2 \mu |\Delta p|^\phi} \right), \quad (25b)$$

$$\lambda_m = \mu |\Delta p|^{t_3} g_{3,\pm} \left( \frac{\kappa}{a^2 \mu |\Delta p|^\phi} \right), \quad (25c)$$

where

$$\phi = 2, \quad (26a)$$

$$t_1 = 1, \quad (26b)$$

$$t_2 = 2, \quad (26c)$$

$$t_3 = 3, \quad (26d)$$

and

$$g_{1,\pm}(x) \simeq \frac{3}{2} \left( \pm 1 + \sqrt{1 - \frac{4\mathcal{A}}{9}x} \right), \quad (27a)$$

$$g_{2,\pm}(x) \simeq \frac{1}{3}x, \quad (27b)$$

$$g_{3,\pm}(x) \simeq \frac{\mathcal{B}}{27} \left( \pm 1 + \sqrt{1 - \frac{4\mathcal{A}}{9}x} \right)^{-1} x^2, \quad (27c)$$

where  $\mathcal{A} \simeq 2.413$  and  $\mathcal{B} \simeq 1.520$  are constants evaluated in App. B. These scaling relations are analogous to that found in random resistor networks with two different types of resistors [38], and central force spring networks with strong and weak springs [37].

Plots of the numerical results in these scaling forms are shown in Fig. 6 along with the above analytical result. These scaling relations can also be expressed in terms of the mean filament length  $\langle L \rangle = 1/(1-p)$  thus  $\langle L \rangle_{CF} = 3$

and  $|p - p_{CF}| \propto |\langle L \rangle - \langle L \rangle_{CF}|$ . Thus, the scaling exponents for functions expressed in terms of  $\langle L \rangle$  are the same as those expressed in terms of  $p$ .

Macroscopic elasticity of the effective medium can be described by the Lamé coefficients, which are both linearly related to  $\mu_m$ , as we discussed in Eq. (7). Thus, the asymptotic forms of  $\mu_m$  can characterize different elastic regimes of the diluted lattice:

$$\begin{aligned} \mu_m &= \mu |\Delta p| \frac{3}{2} \left( \pm 1 + \sqrt{1 - \frac{4\mathcal{A}}{9} \frac{\kappa}{a^2 \mu |\Delta p|^\phi}} \right) \\ &\simeq \begin{cases} \frac{\sqrt{\mathcal{A}}}{a} \mu^{1/2} \kappa^{1/2} & \text{if } \frac{\kappa}{a^2 \mu |\Delta p|^\phi} \gg 1, \\ 3\mu |\Delta p| & \text{if } \frac{\kappa}{a^2 \mu |\Delta p|^\phi} \ll 1 \text{ and } \Delta p > 0, \\ \frac{\mathcal{A}}{3a^2} \frac{\kappa}{|\Delta p|} & \text{if } \frac{\kappa}{a^2 \mu |\Delta p|^\phi} \ll 1 \text{ and } \Delta p < 0. \end{cases} \end{aligned} \quad (28)$$

These crossover regimes correspond exactly to those found in Ref. [37] using known behavior of the density of states and mode structure of systems near the CF isostatic limit and general scaling arguments.

Thus, it is straightforward to see that above the crossover regime, the macroscopic elastic moduli are proportional to  $\mu$ , indicating that the elasticity of the network is dominated by stretching energies, whereas below the crossover regime, the moduli are proportional to  $\kappa$ , indicating that the network elasticity is dominated by bending energies, in agreement with the fact that the system is below the central force isostatic point. Interestingly, in the crossover regime near  $p_{CF}$ , the macroscopic elastic moduli is proportional to  $\mu^{1/2} \kappa^{1/2}$ , corresponding to strong coupling between both stretching and bending modes.

These observations indicate a phase diagram as shown in Fig. 1. There is a rigidity transition between the state with no rigidity (vanishing elastic moduli) and rigid state at  $p_b$ . Above this rigidity transition and at small filament bending stiffness  $\kappa$ , the elasticity of the diluted filamentous lattice is controlled by a crossover at the central force isostatic point  $p_{CF}$ . For large bending stiffness ( $\kappa \sim \mu a^2$ ) the system directly enters the stretching dominated affine elastic regime as  $p$  is increased.

## V. DISCUSSION

Two other approaches produce results similar to ours, and we briefly review compare them to ours.

In references [34] and [36], Das *et al.* present an alternative EMT for systems with both stretching and bending forces. The first of these reference fails to identify either the new rigidity threshold at  $p_b$  and the wide bend-stretch crossover regime near  $p_{CF}$ , but the second does. Stretching forces are easily described by CF springs, which reside on bonds, each of which can have a distinct spring constant, whereas bending forces effectively reside on *phantom* *NNN* bonds. Because removing one *NN* bond from a pair defining a phantom *NNN* bending bond effectively removes that phantom bond,

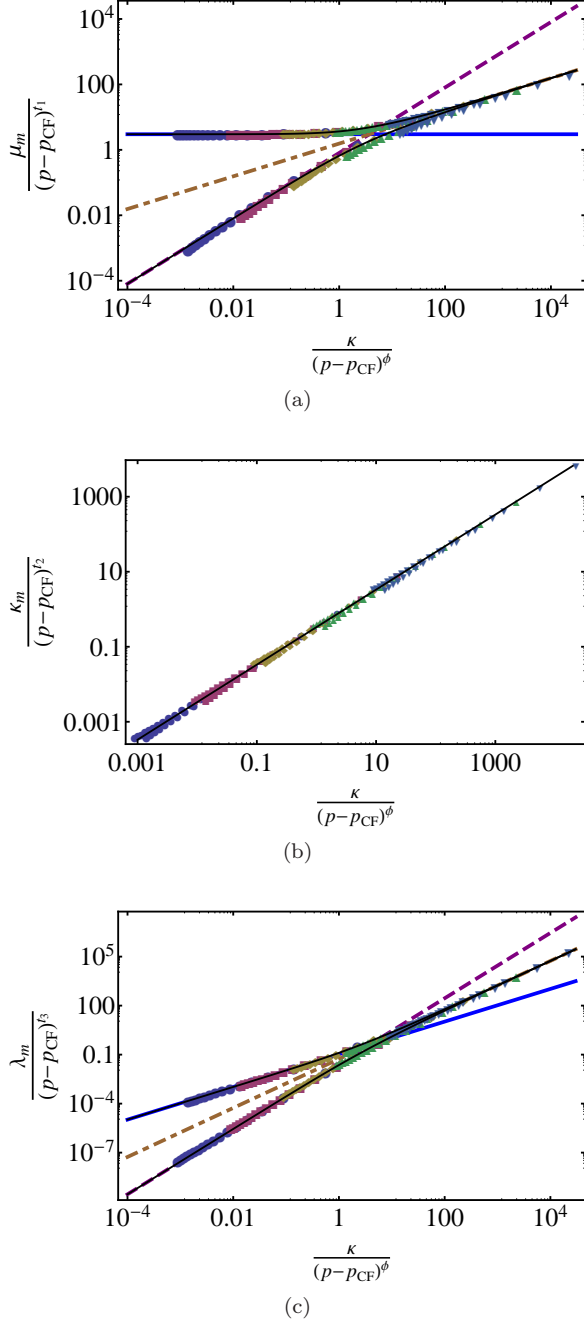


FIG. 6: (color online) (a), (b), and (c) show rescaled plots of the EMT solutions  $\mu_m$ ,  $\kappa_m$  and  $\lambda_m$  using the scaling forms (25a) for  $\mu = 1$  and  $\kappa = 10^{-2}, 10^{-3}, 10^{-4}, 10^{-5}, 10^{-6}$ , with color code the same as in Fig. 3, and exponents taking the value as in Eq. (26a). The thin black lines represent the asymptotic forms (27a) for small  $\kappa$  as solved in App. B. The brown dash-dotted lines, the thick blue solid lines, and the purple dashed lines plot the functional form of  $\mu_m$  obtained in the crossover, the stretching-dominated, and the bending-dominated regimes of Eq. (28), respectively.

bending and stretching are not independent in the diluted lattice. This presents real challenges for the development of a consistent bend-stretch EMT. Our approach to this problem appeals to the underlying polymer nature of our model in which constituent polymers are endowed with local stretching and bending moduli  $\mu$  and  $\kappa$ . We can modify these moduli along any bond. Different stretch moduli lead to independent effective CF stretch force constants  $k_{||}$  for each bond. Modification of the bending modulus  $\kappa$  on a given  $NN$  bond, however, modifies the bend force constant  $k_{\perp}$  for *both* phantom  $NNN$  bonds that that  $NN$  bond partially defines in the manner described above. With this approach, we develop a consistent EMT that includes the statistical correlation between bend and stretch. Das *et al.* ignore this correlation and assume that a stretch spring on a given  $NN$  bond can be removed without affecting the bending energy on the phantom  $NNN$  bonds that include that  $NN$  bond and that bending springs on the phantom  $NNN$  bonds can be removed without affecting the stretch springs on the two bonds that define the  $NNN$  bond. In other words, the phantom bond is effectively elevated to a real bond with existence independent of the underlying  $NN$  bonds. In general, the  $NNN$  bonds can be present with an arbitrary probability  $q$  and absent with probability  $1 - q$ . To provide an approximate description of the constraint that the phantom bond does not exist unless both of the  $NN$  bonds defining it are present, Das *et al.* assign a probability  $q = p^2$  ( $p$  is the probability that a  $NN$  bond is occupied) to the occupancy of a  $NNN$  bending bond, but continue to treat the  $NN$  and  $NNN$  bonds as statistically independent. Again the result is a set of closed self-consistent equations for  $\mu_m$  and  $\kappa_m$ . Both approaches yield  $p_{\text{CF}} = 2/3$  in good agreement with simulations [35], which yield  $p_{\text{CF}} = 0.651$ . Our approach yields a value for  $p_b$  (0.56) that is well above that (0.445) observed in simulations [35] whereas that of Ref. [36] yields a value ( $p_b = 0.4$ ) in good agreement with simulations. Both approaches yield a nontrivial bend-stretch crossover in the vicinity of  $p_{\text{CF}}$  in qualitative agreement with simulations. Our approach gives values of the shear modulus in the crossover region of the same order of magnitude as seen in simulations whereas that of Ref. [36] finds values 1.5 to 2 orders of magnitude higher at small values of  $\kappa$ .

In Ref. [37], Wyart *et al.* consider random off-lattice elastic networks derived from two-dimensional packings of spheres [48] with a coordination number above the Maxwell CF isostatic limit of  $z = 4$  in which CF springs are assigned to each sphere-sphere contact. They use numerical simulations to study the nonlinear relation between shear stress  $\sigma$  and shear strain  $\gamma$  as springs are cut, thereby reducing  $z$ , and they find a scaling relation  $\sigma = \gamma |\delta z| f(\gamma/|\delta z|)$ , where  $\delta z = z - 4$ ,  $f(x) \rightarrow \text{const.}$  for  $x \rightarrow 0^+$ ,  $f(x) \rightarrow 0$  for  $x \rightarrow 0^-$ , and  $f(x) \sim x$  for  $x \rightarrow \infty$ . This scaling form predicts  $\sigma \sim \gamma$  for  $\delta z \gg \gamma > 0$ ,  $\sigma = 0$  for  $\delta z \ll -\gamma < 0$ , and  $\sigma \sim \gamma^2$  for  $\gamma \gg \delta z$ . Reference [37] then provides a theoretical justification for this behavior based upon the existence of a plateau in the density of



states [49] above  $\omega^* \sim \delta z$  and reasonable assumptions about statistical independence of eigenvectors associated with different normal modes in the isostatic network [50] and about the nature of nonaffine response of nearly isostatic systems. Finally, they extend this line of reasoning to nearly isostatic systems with extra weak bonds and find three regimes of elastic response that are identical to those we identify in Eqs. (25a) to (27a) if the weak bonds are of a bending type.

To summarize we developed a new effective-medium theory that can include bending energy of filaments, and we used it to study the development of rigidity of a randomly diluted triangular lattice with central force springs on occupied bonds and bending forces between occupied bond pairs along a straight line. We obtained a rigidity threshold for positive bending stiffness and a crossover, controlled by the isostatic point of the central force triangular lattice, characterizing bending-dominated, stretching-dominated, and stretch-bend coupled elastic regimes.

*Acknowledgments*—We are grateful to C. P. Broedersz and F.C. MacKintosh for many stimulating and helpful discussions. This work was supported in part by NSF-DMR-0804900.

## Appendix A: Bending of a composite rod

In this Appendix we solve for the effective bending rigidity of a composite rod. We solve this problem using a simple setup shown in Fig. 7. We assume that there is a bond of bending rigidity  $\kappa_1$  connecting points  $\ell\ell'$ , and a bond of bending rigidity  $\kappa_2$  connecting points  $\ell'\ell''$ , with points  $\ell, \ell', \ell''$  hold in positions

$$\{-1, h_0\}, \quad \{0, 0\}, \quad \{1, h_0\}, \quad (\text{A1})$$

respectively in space, without losing generality. We then calculate the shape of the bonds which minimize the elastic energy given these fixed end points, treating the bonds as elastic rods. In addition we assume that the stretching stiffness is much greater than the bending stiffness so we can ignore the length change of the bonds. The elastic energy of a bond is then simply the bending energy of a rod with bending stiffness  $\kappa$

$$E = \frac{\kappa}{2} \int dx \left[ \frac{d^2 h(x)}{dx^2} \right]^2 \quad (\text{A2})$$

where we have assumed small deformations so the elastic energy takes the form of an expansion in small  $h(x)$ . The variational condition that a configuration minimizes this elastic energy is

$$\frac{d^4 h(x)}{dx^4} = 0. \quad (\text{A3})$$

Therefore, we can assume the shape of the two bonds

$$\begin{aligned} h(x) &= Ax + \frac{1}{2}B_1x^2 + \frac{1}{6}C_1x^3 \quad \text{for } x < 0 \\ h(x) &= Ax + \frac{1}{2}B_2x^2 + \frac{1}{6}C_2x^3 \quad \text{for } x > 0 \end{aligned} \quad (\text{A4})$$

where the first line corresponds to the bond between  $\ell\ell'$ , and the second line correspond to the bond between  $\ell'\ell''$ . This form already satisfies the condition that the two bonds are connected and smooth at their conjunction  $x = 0$ . We have two boundary conditions at  $x = -1$  and  $x = 1$

$$\begin{aligned} h_0 &= -A + \frac{1}{2}B_1 - \frac{1}{6}C_1 \\ h_0 &= A + \frac{1}{2}B_2 + \frac{1}{6}C_2. \end{aligned} \quad (\text{A5})$$

Under these boundary conditions we minimize the total elastic energy of the two bonds

$$\begin{aligned} E &= \frac{\kappa_1}{2} \int_{-1}^0 dx \left[ \frac{d^2 h(x)}{dx^2} \right]^2 + \frac{\kappa_2}{2} \int_0^1 dx \left[ \frac{d^2 h(x)}{dx^2} \right]^2 \\ &= \frac{\kappa_1}{2} \left( B_1^2 - B_1C_1 + \frac{C_1^2}{3} \right) \\ &\quad + \frac{\kappa_2}{2} \left( B_2^2 + B_2C_2 + \frac{C_2^2}{3} \right). \end{aligned} \quad (\text{A6})$$

This calculation leads to the minimum elastic energy

$$E_m = \frac{6\kappa_1\kappa_2h_0^2}{\kappa_1 + \kappa_2}. \quad (\text{A7})$$

In the above calculation, if we assumed that both of the two bonds are of bending stiffness  $\kappa_{\text{eff}}$ , we get

$$E_m = 3\kappa_{\text{eff}}h_0^2. \quad (\text{A8})$$

Therefore we arrive at the effective bending stiffness of the composite rod

$$\kappa_{\text{eff}} = \frac{2\kappa_1\kappa_2}{\kappa_1 + \kappa_2}. \quad (\text{A9})$$

which reduces to  $\kappa_1$  if  $\kappa_1 = \kappa_2$  as we expected.

## Appendix B: Asymptotic solution of the CPA self consistency equation near $p_{\text{CF}}$

In this Appendix we solve the EMT self-consistency equation [Eq. (20)] asymptotically near  $p_{\text{CF}}$  at small  $\kappa$ . In the zeroth order,  $\kappa = 0$ , and the problem reduces to that of a central force rigidity percolation. We expand the equation around this point and solve for the effective-medium spring constants asymptotically in small  $\kappa$ .

To obtain the asymptotic solution, we rewrite the EMT self-consistency equation [Eq. (20)] as

$$p\tilde{\mathbf{V}}(\mu, \kappa) + (1-p)\tilde{\mathbf{V}}(0, 0) - \tilde{\mathbf{V}}(0, 0)\tilde{\mathbf{G}}\tilde{\mathbf{V}}(\mu, \kappa) = 0, \quad (\text{B1})$$

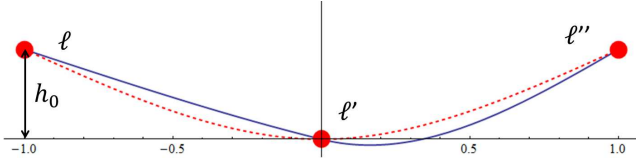


FIG. 7: (Color online) Bending of the composite rod. The 3 red disks mark the fixed end points of the two bonds. The blue solid line represent the shape of the two bonds solved for the case of  $\kappa_1 = 10\kappa_2$ , and the red dashed line represent the shape of the two bonds for the case of  $\kappa_1 = \kappa_2$  which is symmetric under  $x \rightarrow -x$ .

to avoid the apparent singularity in  $\tilde{\mathbf{V}}^{-1}$  at the point

$\kappa = 0$ .

It is straightforward to see from the symmetry of  $\tilde{\mathbf{V}}^{-1}$  and  $\tilde{\mathbf{G}}$  as in Eqs. (16) and (22) that the matrix equation [Eq. (20)] contains 3 independent equations. The 11-element gives

$$\mu_m = \mu \frac{p - H_1(b_m, l_m)}{1 - H_1(b_m, l_m)}. \quad (\text{B2})$$

To zeroth order,  $\kappa = 0$ , we obtain  $H_1(0, 0) = p_{\text{CF}} = 2d/z = 2/3$  from the fact that all bonds are equivalent, and Eq. (B2) reduces to the EMT equation for central-force rigidity percolation.

The 22- and 23-elements of the matrix equation (20) read

$$2\left(\frac{1}{b} + \frac{1}{b_m}\right)^{-1} \left(p - \frac{1}{2}\left(1 + \frac{b_m}{b}\right) - b_m H_2 - l_m H_3\right) + (b_m^2 + l_m^2) H_2 + 2b_m l_m H_3 = 0, \quad (\text{B3})$$

$$-l_m - 2\left(\frac{1}{b} + \frac{1}{b_m}\right)^{-1} (l_m H_2 + b_m H_3) + 2b_m l_m H_2 + (b_m^2 + l_m^2) H_3 = 0, \quad (\text{B4})$$

where  $b \equiv \kappa/(\mu_m a^2)$ ,  $H_2(b_m, l_m)$  and  $H_3(b_m, l_m)$  are the 22 and 23 elements of  $H(b_m, l_m)$  respectively. Thus we have 3 unknowns  $\{\mu_m, b_m, l_m\}$  (or equivalently,  $\{\mu_m, \kappa_m, \lambda_m\}$ ) and 3 equations (B2), (B3), and (B4). As we already discussed, at  $\kappa = 0$ , the zeroth order solution is  $\{\mu_m^{(0)} = \mu \frac{p - p_{\text{CF}}}{1 - p_{\text{CF}}}, b_m^{(0)} = 0, l_m^{(0)} = 0\}$ , where  $p_{\text{CF}} = H_1(0, 0)$ . Notice that the equations up to this point are all exact within the EMT.

As  $\kappa$  becomes positive,  $\mu_m$  increases,  $b_m$  and  $l_m$  become nonzero, and the rigidity threshold jumps to a lower value  $p_b$  as shown in Fig. 3(b). For small  $\kappa$ , we have  $\kappa/(\mu a^2) \ll 1$ , and can assume that  $b_m, l_m \ll 1$  (which we will verify later), and we find that to the leading order the 3 Eqs. (B2), (B3), and (B4) become

$$\mu_m \simeq \mu \frac{p - p_{\text{CF}} - H_{1,1}(0, 0) \kappa_m / (\mu_m a^2)}{1 - p_{\text{CF}}}, \quad (\text{B5a})$$

$$\kappa_m \simeq \kappa(2p - 1), \quad (\text{B5b})$$

$$\lambda_m \simeq \kappa H_3(0, 0) \frac{\kappa}{\mu_m a^2} \frac{1 - p}{p} (2p - 1)^2, \quad (\text{B5c})$$

where  $H_{1,1}(0, 0) = \partial H_1 / \partial b_m|_{b_m=0, l_m=0} \simeq -2.413$  and  $H_3(0, 0) = 1.520$ . From these relations, we find that at  $p = p_{\text{CF}}$

$$\mu_m \sim \kappa^{1/2}, \quad (\text{B6a})$$

$$\kappa_m \sim \kappa, \quad (\text{B6b})$$

$$\lambda_m \sim \kappa^{3/2}, \quad (\text{B6c})$$

indicating that  $\mu_m \gg \kappa_m \gg \lambda_m$  and thus  $b_m, l_m \ll 1$  as we assumed. Using these relations, together with the fact that as  $\kappa \rightarrow 0$ ,  $\mu_m \rightarrow p - p_{\text{CF}}$ , we arrive at the scaling relations

$$\mu_m = \mu |\Delta p| g_{1,\pm} \left( \frac{\kappa}{a^2 \mu |\Delta p|^2} \right), \quad (\text{B7a})$$

$$\kappa_m = \mu a^2 |\Delta p|^2 g_{2,\pm} \left( \frac{\kappa}{a^2 \mu |\Delta p|^2} \right), \quad (\text{B7b})$$

$$\lambda_m = \mu a^2 |\Delta p|^3 g_{3,\pm} \left( \frac{\kappa}{a^2 \mu |\Delta p|^2} \right), \quad (\text{B7c})$$

where  $\Delta p \equiv p - p_{\text{CF}}$ . These scaling forms agree well with our numerical solutions (See Fig. 6).

From Eq. (B5), we can further solve for the form of these scaling functions

$$g_{1,\pm}(x) \simeq \frac{3}{2} \left( \pm 1 + \sqrt{1 - \frac{4\mathcal{A}}{9}x} \right), \quad (\text{B8a})$$

$$g_{2,\pm}(x) \simeq \frac{1}{3}x, \quad (\text{B8b})$$

$$g_{3,\pm}(x) \simeq \frac{\mathcal{B}}{27} \left( \pm 1 + \sqrt{1 - \frac{4\mathcal{A}}{9}x} \right)^{-1} x^2 \quad (\text{B8c})$$

with  $\mathcal{A} \equiv -H_{1,1}(0,0)$  and  $\mathcal{B} \equiv H_3(0,0)$ . These scaling forms with  $H_{1,1}$  and  $H_3$  obtained numerically are plotted together with the numerical solutions in Fig. 6 in nice agreement.

These scaling functions can be expanded in different limits. In particular, for the effective medium stretching stiffness  $\mu$ , which is closely related to the macroscopic elastic moduli, we have

$$g_{1,\pm}(x) \simeq \begin{cases} \sqrt{\mathcal{A}}\sqrt{x} & \text{if } x \gg 1, \\ 3 & \text{if } x \ll 1 \text{ and } \Delta p > 0, \\ \frac{1}{3}\mathcal{A}x & \text{if } x \ll 1 \text{ and } \Delta p < 0, \end{cases} \quad (\text{B9})$$

indicating different elastic regimes as we discussed in Sec.III.

### Appendix C: Asymptotic solution of the CPA self consistency equation near $p_b$

Equations (B2,B3,B4) can also be used to solve for the asymptotics near the rigidity threshold  $p_b$ . In particular, because  $l_m, b_m$  converge to constants that are much smaller than unity and independent of  $\kappa$  near  $p_b$ , the asymptotic solution near  $p_b$  in this section are not limited to small  $\kappa$ .

Firstly we solve for the value of the rigidity threshold  $p_b$  for the case of  $\kappa > 0$  using these EMT equations. At  $p_b$ , we have  $\mu_m = 0, \kappa_m = 0, \lambda_m = 0$  and as a result  $b \rightarrow \infty$ , and we solve for  $p_b, b_m, l_m$ . So the equations determine  $p_b, b_m = b_b, l_m = l_b$  are

$$\begin{aligned} p_b - H_1(b_b, l_b) &= 0, \\ 2b_b \left( p_b - \frac{1}{2} \right) + (-b_b^2 + l_b^2) H_2(b_b, l_b) &= 0, \\ -l_b + (-b_b^2 + l_b^2) H_3(b_b, l_b) &= 0, \end{aligned} \quad (\text{C1})$$

where  $b_b$  and  $l_b$  are the value of  $b_m$  and  $l_m$  at  $p_b$ . This set of equations is independent of  $\kappa$ . Numerical solution to these equations are given by

$$\begin{aligned} p_b &\simeq 0.5584, \\ b_b &\simeq 0.06355, \\ l_b &\simeq 0.004235, \end{aligned} \quad (\text{C2})$$

which agrees with the results we obtained by solving the EMT equations numerically.

Secondly we solve for the asymptotic behaviors near  $p_b$ . To achieve this, we suppose  $p = p_b + \delta p$ , and to first order we have

$$\begin{aligned} \mu_m &= 0 + \delta \mu_m \\ b_m &= b_b + \delta b_m \\ l_m &= l_b + \delta l_m. \end{aligned} \quad (\text{C3})$$

We put these expansions back into Eqs. (B2,B3,B4) we get the first order perturbation equations

$$\delta \mu_m = \mu \frac{\delta p - A_1 \delta b_m - A_2 \delta l_m}{1 - p_b}, \quad (\text{C4})$$

$$(2p_b - 1 - 2b_b H_{2,0}) \delta b_m = -2b_b \delta p + 2p_b b_b^2 \frac{\delta \mu_m a^2}{\kappa}, \quad (\text{C5})$$

$$\delta l_m = -2b_b H_{3,0} \delta b_m. \quad (\text{C6})$$

In deriving these equations we used the fact that  $l_b \ll b_b \ll 1$  and  $\frac{b_m}{b} = \frac{\kappa_m}{\kappa} \ll 1$  near  $p_b$ . Thus we arrive at the asymptotic solution of the effective medium stretching stiffness

$$\mu_m = \mu \frac{c_2 \delta p}{1 + c_1 \frac{a^2 \mu}{\kappa}} \quad (\text{C7})$$

where

$$\begin{aligned} c_1 &= \frac{A_1 - 2b_b H_{3,0} A_2}{2p_b - 1 - 2b_b H_{2,0}} \frac{2p_b b_b^2}{1 - p_b} \\ c_2 &= \frac{1}{1 - p_b} \left( 1 + 2b_b \frac{A_1 - 2b_b H_{3,0} A_2}{2p_b - 1 - 2b_b H_{2,0}} \right) \end{aligned} \quad (\text{C8})$$

are constants determined by the architecture of the lattice and are independent of  $p$  or  $\kappa/(\mu a^2)$ . In the case of triangular lattice we have  $c_1 = 0.1018$  and  $c_2 = 5.132$ .

### Appendix D: Estimates of the rigidity threshold using Maxwell counting of floppy modes

In this appendix, we use Maxwell counting [5, 6, 24] of the number of floppy modes to estimate the rigidity threshold of a filamentous triangular lattice. Bending forces cause bending excitations on a single filament to have nonzero frequency. Thus in the counting of zero modes, we can treat each filament as a rigid rod with two translational and one rotational degree of freedom.

Thus the number of floppy modes in the network is given by

$$N_0 = 3N_f - N_c \quad (D1)$$

where  $N_f$  is the total number of filaments and  $N_c$  is the total number of constraints in the network. Upon dilution,  $N_f$  increases and  $N_c$  decreases, and thus  $N_0$  becomes positive at the threshold occupancy probability  $p_b$ .

To calculate the number of filaments  $N_f$ , we use the fact that the average length of the filaments is [35]

$$\langle L \rangle = \frac{1}{1-p}. \quad (D2)$$

Consider a straight line in the lattice (which would be one whole filament if  $p = 1$ ) with  $N_b$  bonds, the mean number of filaments in this line  $N_f$  satisfies the equation

$$N_f \langle L \rangle = p N_b. \quad (D3)$$

Thus we get the mean number of filaments *per lattice site*

$$n_f = 3p(1-p). \quad (D4)$$

The number of constraints at a crosslink where 2 filaments meet is 2, because the crosslink puts the constraint on the 2 filaments that the linked sites on these 2 filaments have to move together in both  $x$  and  $y$  directions. The number of constraints at a crosslink where 3 filaments meet is 4 correspondingly. Thus for occupancy probability  $p$  of the bonds, the mean number of constraints *per lattice site* is given by

$$\begin{aligned} n_c = & 4p^6 + 4 \times 6p^5(1-p) \\ & + (4 \times 12 + 2 \times 3)p^4(1-p)^2 \\ & + (4 \times 8 + 2 \times 12)p^3(1-p)^3 \\ & + 2 \times 12p^2(1-p)^4, \end{aligned} \quad (D5)$$

with the terms illustrated in Fig. 8.

From the equation of floppy modes *per lattice site*

$$3n_f - n_c = 0 \quad (D6)$$

we obtain the rigidity threshold

$$p_b = 0.4475, \quad (D7)$$

which is very close to the value obtained in numerical simulation of filamentous triangular network [35].

This estimation of the rigidity threshold can also be applied to other cases. For example, we consider the two dimensional kagome lattice, which has  $z = 4$  when undiluted. Thus the  $p = 1$  point is the CF isostatic point. In the presence of bending forces, we follow a similar calculation and get

$$\begin{aligned} n_f &= 2p(1-p), \\ n_c &= 2p^4 + 2 \times 4p^3(1-p) + 2 \times 4p^2(1-p)^2. \end{aligned} \quad (D8)$$

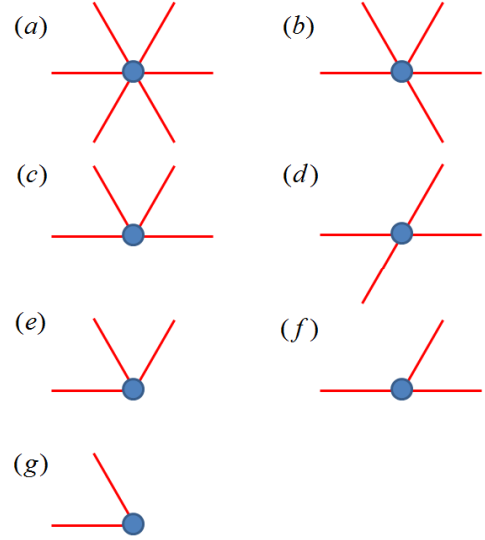


FIG. 8: Illustration of the configurations of bonds connecting to a site for given probability  $p$ , corresponding to terms in Eq. (D5) (only one diagram is shown for each type of configurations with the same probability and the same number of constraints). From (a) through (g) the probability and the number of constraints are respectively  $(p^4, 4)$ ,  $(6p^5(1-p), 4)$ ,  $(12p^4(1-p)^2, 4)$ ,  $(3p^4(1-p)^2, 2)$ ,  $(8p^3(1-p)^3, 4)$ ,  $(12p^3(1-p)^3, 2)$ ,  $(12p^2(1-p)^4, 2)$ . The rest of the possible configurations, such as only two bonds along a line or only one bond connected to the site does not contribute constraints.

Thus the rigidity threshold with bending forces is at

$$p_b = 0.6074. \quad (D9)$$

Another example we consider is the three dimensional filamentous face centered cubic (FCC) lattice. The undiluted FCC lattice has  $z = 12$  and is well above isostaticity, similar to the case of triangular lattice.  $n_f$  and  $n_c$  for the FCC lattice is given by

$$\begin{aligned} n_f &= 6p(1-p), \\ n_c &= 3[5p^{12} + 5 \times 12p^{11}(1-p) \\ &+ (5 \times 60 + 4 \times 6)p^{10}(1-p)^2 \\ &+ (5 \times 160 + 4 \times 60)p^9(1-p)^3 \\ &+ (5 \times 240 + 4 \times 240 + 3 \times 15)p^8(1-p)^4 \\ &+ (5 \times 192 + 4 \times 480 + 3 \times 120)p^7(1-p)^5 \\ &+ (5 \times 64 + 4 \times 480 + 3 \times 360 + 2 \times 20)p^6(1-p)^6 \\ &+ (4 \times 192 + 3 \times 480 + 2 \times 120)p^5(1-p)^7 \\ &+ (3 \times 240 + 2 \times 240 + 1 \times 15)p^4(1-p)^8 \\ &+ (2 \times 160 + 1 \times 60)p^3(1-p)^9 \\ &+ 60p^2(1-p)^{10}]. \end{aligned} \quad (D10)$$

In three dimensions the equation for vanishing floppy modes is

$$5n_f - n_c = 0 \quad (D11)$$

and we get the rigidity threshold for FCC lattice at

$$p_b \simeq 0.3062. \quad (D12)$$

- 
- [1] A. J. Liu and S. R. Nagel, *Nature* **396**, 21 (1998).
  - [2] M. Wyart, *Ann. Phys. Fr* **30**, 1 (2005).
  - [3] A. J. Liu and S. R. Nagel, in *Annual Review of Condensed Matter Physics* (2010), vol. 1, pp. 347–369.
  - [4] J. C. Phillips, *J. Non-Cryst. Solids* **43**, 37 (1981).
  - [5] M. Thorpe, *J. Non-Cryst. Solids* **57**, 355 (1983).
  - [6] J. C. Phillips and M. F. Thorpe, *Solid State Commun.* **53**, 699 (1985).
  - [7] H. He and M. F. Thorpe, *Phys. Rev. Lett.* **54**, 2107 (1985).
  - [8] M. Thorpe, D. Jacobs, M. Chubynsky, and J. Phillips, *J. Non-Cryst. Solids* **266**, 859 (2000).
  - [9] E. Elson, *Annu. Rev. Biophys. Chem.* **17**, 397 (1988).
  - [10] K. Kasza, A. Rowat, J. Liu, T. Angelini, C. Brangwynne, G. Koenderink, and D. Weitz, *Curr. Opin. Cell Biol.* **19**, 101 (2007).
  - [11] B. Alberts, A. Johnson, J. Lewis, M. Raff, K. Roberts, and P. Walter, *Molecular Biology of the Cell* (Garland, New York, 2008), 4th ed.
  - [12] P. Janmey, S. Hvidt, J. Lamb, and T. Stossel, *Nature* **345**, 89 (1997).
  - [13] F. C. MacKintosh, J. Käs, and P. A. Janmey, *Phys. Rev. Lett.* **75**, 4425 (1995).
  - [14] D. A. Head, A. J. Levine, and F. C. MacKintosh, *Phys. Rev. Lett.* **91**, 108102 (2003).
  - [15] J. Wilhelm and E. Frey, *Phys. Rev. Lett.* **91**, 108103 (2003).
  - [16] D. A. Head, A. J. Levine, and F. C. MacKintosh, *Phys. Rev. E* **72**, 061914 (2005).
  - [17] C. Storm, J. Pastore, F. MacKintosh, T. Lubensky, and P. Janmey, *Nature* **435**, 191 (2005).
  - [18] P. R. Onck, T. Koeman, T. van Dillen, and E. van der Giessen, *Phys. Rev. Lett.* **95**, 178102 (2005).
  - [19] E. M. Huisman, T. van Dillen, P. R. Onck, and E. Van der Giessen, *Phys. Rev. Lett.* **99**, 208103 (2007).
  - [20] E. M. Huisman and T. C. Lubensky, *Phys. Rev. Lett.* **106**, 088301 (2011).
  - [21] S. Feng and P. N. Sen, *Phys. Rev. Lett.* **52**, 216 (1984).
  - [22] S. Feng, P. N. Sen, B. I. Halperin, and C. J. Lobb, *Phys. Rev. B* **30**, 5386 (1984).
  - [23] D. J. Jacobs and M. F. Thorpe, *Phys. Rev. Lett.* **75**, 4051 (1995).
  - [24] J. C. Maxwell, *Philos. Mag.* **27**, 294 (1864).
  - [25] C. Calladine, *Int. J. Solids Struct.* **14**, 161 (1978).
  - [26] D. J. Jacobs and M. F. Thorpe, *Phys. Rev. E* **53**, 3682 (1996).
  - [27] P. Soven, *Phys. Rev.* **178**, 1136 (1969).
  - [28] R. J. Elliott, J. A. Krumhansl, and P. L. Leath, *Rev. Mod. Phys.* **46**, 465 (1974).
  - [29] S. Feng, M. F. Thorpe, and E. Garboczi, *Phys. Rev. B* **31**, 276 (1985).
  - [30] E. J. Garboczi and M. F. Thorpe, *Phys. Rev. B* **31**, 7276 (1985).
  - [31] L. M. Schwartz, S. Feng, M. F. Thorpe, and P. N. Sen, *Phys. Rev. B* **32**, 4607 (1985).
  - [32] C. Heussinger and E. Frey, *Phys. Rev. Lett.* **97**, 105501 (2006).
  - [33] C. Heussinger, B. Schaefer, and E. Frey, *Phys. Rev. E* **76**, 031906 (2007).
  - [34] M. Das, F. C. MacKintosh, and A. J. Levine, *Phys. Rev. Lett.* **99**, 038101 (2007).
  - [35] C. P. Broedersz, F. MacKintosh, X. Mao, T. Lubensky, and F. MacKintosh, *arXiv:1011.6535v1 [cond-mat.soft]* (2010).
  - [36] M. Das, D. Quint, and J. Schwarz, *arXiv:1106.3004* (2011).
  - [37] M. Wyart, H. Liang, A. Kabla, and L. Mahadevan, *Phys. Rev. Lett.* **101**, 215501 (2008).
  - [38] J. P. Straley, *J. of Phys. C Solid State* **9**, 783 (1976).
  - [39] M. Latva-Kokko and J. Timonen, *Phys. Rev. E* **64**, 066117 (2001).
  - [40] X. Mao, O. Stenull, and T. C. Lubensky, *Unpublished* (2011).
  - [41] O. Stenull and T. C. Lubensky, *arXiv:1108.4328v1 [cond-mat.soft]* (2011).
  - [42] S. Alexander, *Phys. Rep.* **296**, 65 (1998).
  - [43] P. Boolchand, G. Lucovsky, J. C. Phillips, and M. F. Thorpe, *Philos. Mag.* **85**, 3823 (2005).
  - [44] O. Kratky and G. Porod, *Rec. Trav. Chim. Pays-Bas.* **68** (1949).
  - [45] J. Marko and E. Siggia, *Macromolecules* **28**, 8759 (1995).
  - [46] S. Kirkpatrick, B. Velický, and H. Ehrenreich, *Phys. Rev. B* **1**, 3250 (1970).
  - [47] X. Mao, N. Xu, and T. C. Lubensky, *Phys. Rev. Lett.* **104**, 085504 (2010).
  - [48] C. S. O'Hern, L. E. Silbert, A. J. Liu, and S. R. Nagel, *Phys. Rev. E* **68**, 011306 (2003).
  - [49] L. E. Silbert, A. J. Liu, and S. R. Nagel, *Phys. Rev. Lett.* **95**, 098301 (2005).
  - [50] C. E. Maloney, *Phys. Rev. Lett.* **97**, 035503 (2006).